Supplementary Material for

Cerium-Infused Bismuth Ferrite: A Piezoelectric Powerhouse Igniting Fenton-like Catalysis to Shatter Microplastics

Meixuan Wu[1], Luzhen Bai[2], Si Chen[3], Lin Miao[4], Pengfei Sun[4], Baocheng Zhou[4], Yubing Xiong[4], Xiaoping Dong[*4]

1 School of Materials Science and Engineering, Zhejiang Sci-Tech University, Hangzhou 310018, China.

2 Zhejiang Provincial Energy Group Company Ltd., No.152 Tianmushan Road, Xihu District, Hangzhou 310000, Zhejiang Province, China

3 Institute of Fundamental and Frontier Sciences, University of Electronic Science and Technology of China, Chengdu, 611731, China.

4 School of Chemistry and Chemical Engineering, Key Laboratory of Surface & Interface Science of Polymer Materials of Zhejiang Province, Zhejiang Sci-Tech University, Hangzhou 310018, China.

Corresponding author: xpdong@zstu.edu.cn

Characterizations of Catalysts

X-ray diffraction (XRD) was used to characterize the crystal structure of the catalysts. An X-ray diffractometer model DX-2700 (Dandong Haoyuan Instrument Co., Ltd., China), equipped with a Cu-Kα target as the diffraction source with a characteristic wavelength of 1.5406 Å, was used in the experiments. The scanning voltage and current of the instrument were set to 36 kV and 30 mA, respectively. The microstructure and elemental distribution of the samples were analyzed by scanning electron microscope (SEM, SU8100 Hitachi, Japan) combined with energy dispersive X-ray spectroscopy (EDS). The micro-morphology and crystal micro-structure of the samples were observed using transmission electron microscope (TEM, JEM-2100 JEOL, Japan). Fourier transform infrared (FT-IR) spectra were recorded using a Nicolet Avatar 370 spectrophotometer. X-ray

photoelectron spectroscopy (XPS) was conducted using a PHI 5400 spectrometer with a non-monochromatic Mg Kα X-ray source (1253.6 eV, 15 kV, 300 W) and a hemispherical sector analyzer. Advantage software was used to analyze the XPS high-energy resolution spectra. UV-vis diffuse reflectance spectra (DRS) were recorded on a Shimadzu UV-2600 UV-vis spectrophotometer in the 200-800 nm range using $BaSO_4$ as a reference. The piezoelectric response of the sample was studied using piezoelectric response microscopy (PFM) and KPFM with an Oxford Instruments Jupiter XR atomic force microscope equipped with an ASYELEC-01-R2 probe.

Characterizations of MPs

The morphology of the original and degraded PET-MPs was characterized by COXEM EM-30 C desktop scanning electron microscope, and the obtained images were analyzed with Nano-Measure 1.2 software. The chemical structure and functional groups of the PET-MPs were analyzed using attenuated total reflection-Fourier transform infrared spectroscopy (ATR-FTIR), performed on a Nicolette Avatar 370 spectrophotometer. The thermal properties were evaluated by thermogravimetric analysis-differential scanning calorimetry (TGA-DSC) with a Discovery SDT 650 synchronous thermal analyzer from TA Instruments (USA).

DFT calculations

The density functional theory (DFT) calculations were performed via "Vienna ab initio simulation package" (VASP 5.4.1). The DFT+U (U=3.8 eV, U=5.0 eV) was implemented to account for the one-site Coulomb interaction for Fe 3d electrons and Ce 4f, respectively. The magnetism influence of Fe was taken into consideration with ISPIN=2. The cutoff energy and Gaussian smearing width were set to 400 eV and 0.2 eV, respectively. The K point in the Brillouin zone was set to 3*3*1 within the Monkhorst-Pack grid for both structural optimization and electronic structural calculations. The vacuum slab was set to 15 Å to avoid an interaction error between neighboring supercells. The adsorption energy (E_{ads}) was calculated as follows:

$$Eads = E_{tot} (E_{mol} + E_{material})$$

Where E_{tot}, E_{mol} and $E_{material}$ are the total energy of the adsorption system, the isolated molecule and the material structure, respectively.

The Gibbs free energies were calculated at 298.15 K, and as defined as:

$$G = EDFT \cdot TS + EZPE$$

Where EDFT, TS and EZPE refers to the DFT energy, entropy contribution, and zero-point energy, respectively.

Method of electron paramagnetic resonance (EPR)

The active species were detected using EPR experiments with the following parameters: microwave power of 21.61 mW, magnetic field strength of 3500.8 Gs, scanning width of 100 Gs, electrostatic field strength of 3450.81 Gs, microwave frequency of 9.81 GHz, modulation frequency of 100 KHz, modulation amplitude of 1.00 Gs, and scanning time of 30.72 s.

Quantitative analysis of $\cdot O_2^-$ and $\cdot OH$

Nitrotetrazole blue chloride (NBT) reacts with $\cdot O_2^-$ to form a product with a distinctive UV absorption peak at 259 nm. This characteristic allows monitoring of $\cdot O_2^-$ by measuring changes in UV absorbance. To carry out the experiment, prepare 10 mL of 0.55 mg/L NBT solution in each reaction system. Periodically take 1 mL solution from the reaction mixture. Centrifuge each sample to separate it and collect the supernatant. Measure the UV absorbance of the supernatant at 259 nm.

2-Hydroxyterephthalic acid (TAOH), generated from the reaction of terephthalic acid (TA) with ·OH, exhibits strong fluorescence when excited at 315 nm. A 10 mL mixed solution containing 2 mM NaOH and 0.5 mM TA was introduced into the reaction system. Fluorescence spectroscopy revealed a distinct emission peak at 425 nm for the product. This fluorescence intensity was utilized to quantitative determination the concentration of OH produced.

Method of HPLC

A high-performance liquid chromatograph (HPLC) (Thermo Fisher UltiMate 3000) equipped with a Spherisorb ODS2 column (4.6 mm×200 mm) and a UV detector was used to analyze the supernatant obtained after the degradation of PET-MPs. The aim was to preliminarily determine the changes in solution intermediates during the degradation process. The test conditions were as follows: an injection volume of 20 μL, a mobile phase consisting of phosphate (pH adjusted to 2.0 with phosphoric acid) and methanol in a ratio of 70:30, a flow rate of 1 mL/min and detection at 254 nm.

LC-MS analysis

Liquid chromatography-mass spectrometry (LC-MS) analysis of the supernatant was

performed on an Agilent 1100 liquid chromatograph coupled with a TSQ quantum super-mass spectrometer (Thermo Fisher Scientific) in negative electron spray ionization (ESI) scan mode using a WELCH Ultimate C18 column (3 μm, 2.1 mm × 100 mm). The mobile phase flow rate was 0.3 mL/min. The mobile phase A consisted of a mixture of 0.1% formic acid aqueous solution and methanol (95:5), while mobile phase B was a methanol solution containing 0.1% formic acid. During the initial 8 min, the proportion of component A was progressively decreased from 90% to 2%. Following a 3 min period of steady flow at 2% A, the proportion of A was then gradually increased back to its initial level of 90% over the subsequent 3 min.

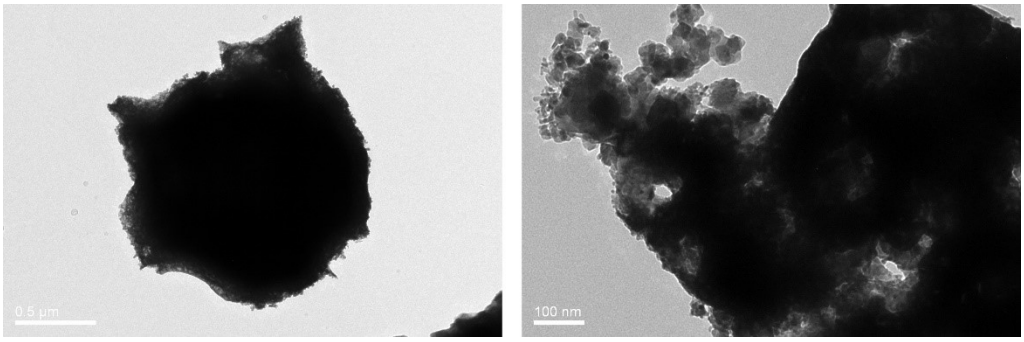

Fig. S1 TEM images of BCFO its edge.

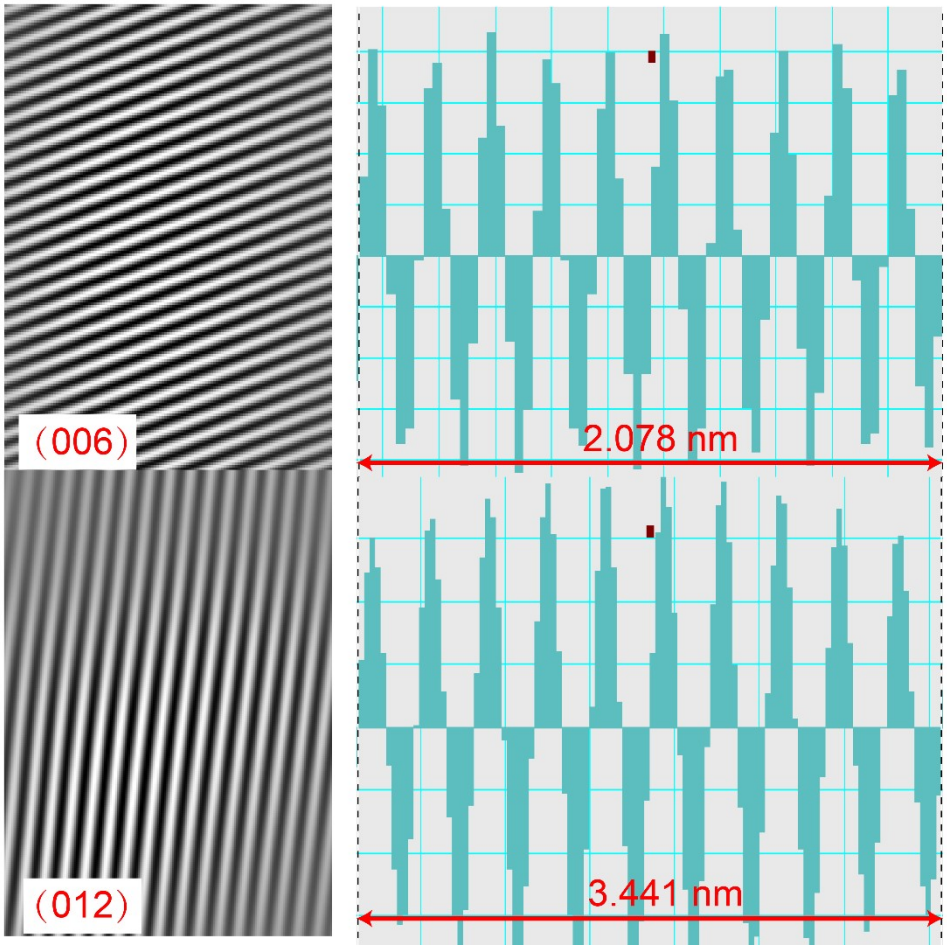

Fig. S2 The spacings of (006) and (012) crystal planes.

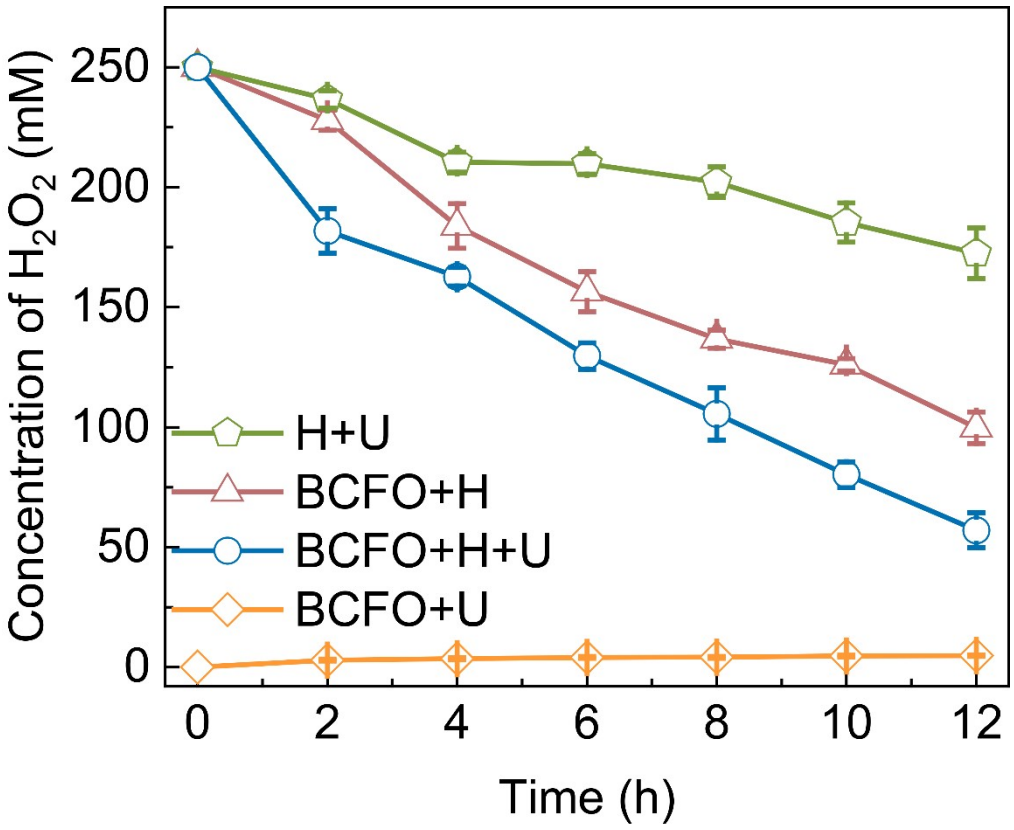

Fig. S3 H_2O_2 consumption/formation rate under differentconditions.

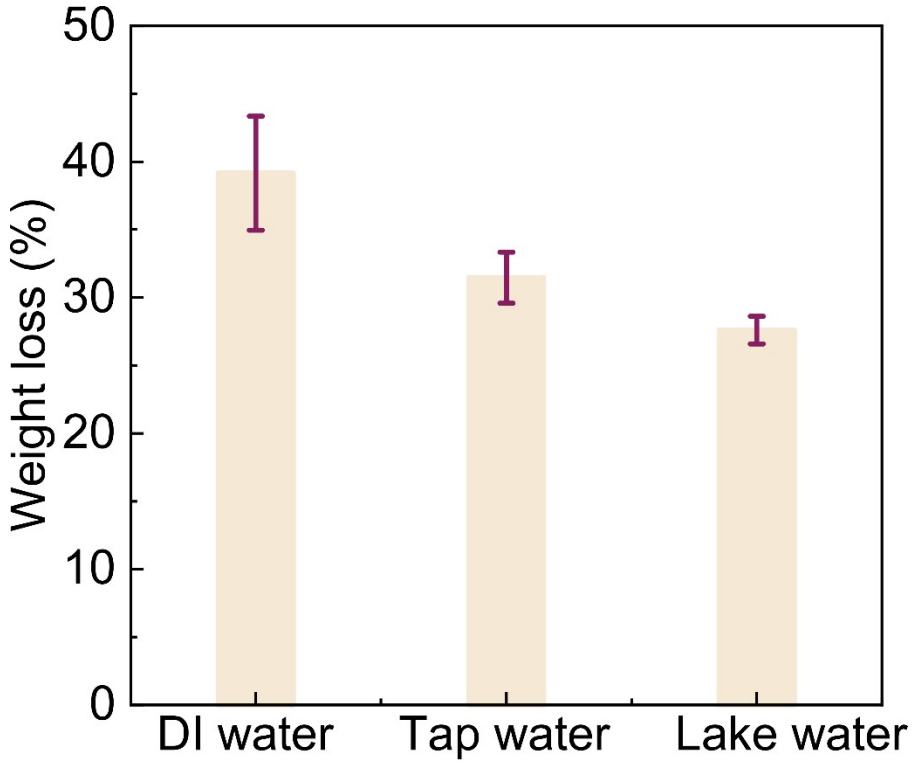

Fig. S4 Weight loss efficiency of PET-MPs in different water bodies.

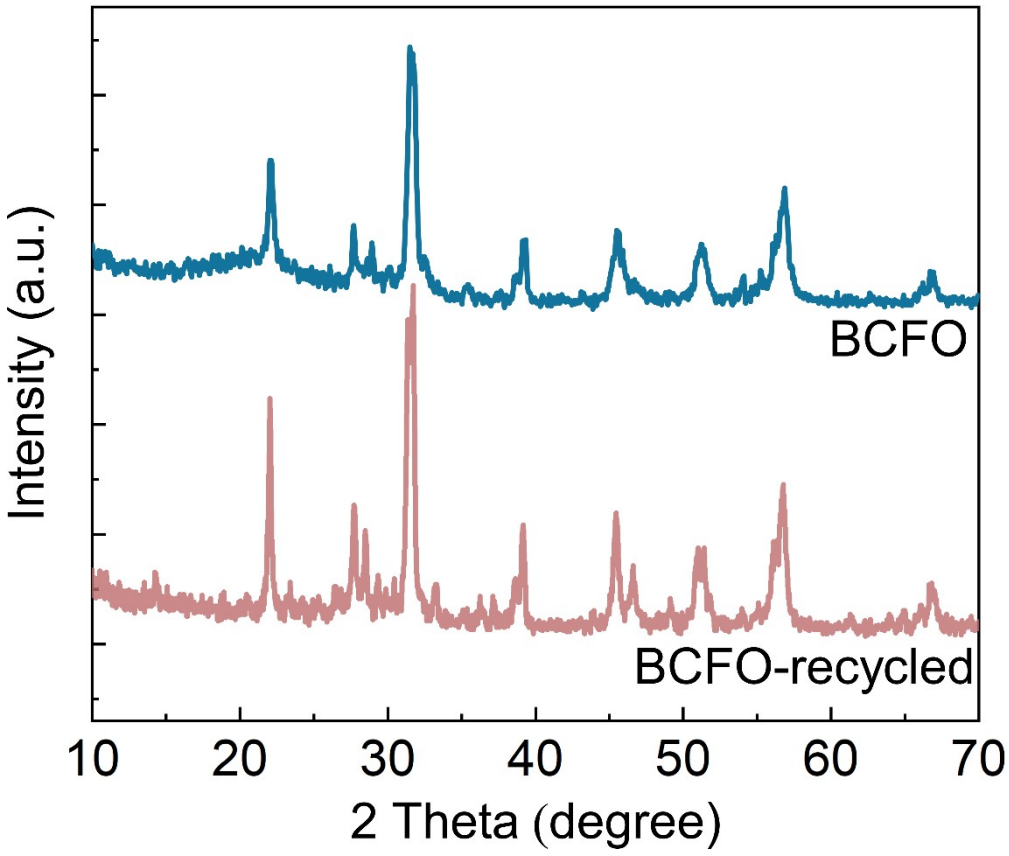

Fig. S5 XRD patterns of fresh and recycled BCFO.

Table S1 Comparison with other degradation systems from recent works for PET MPs degradation.

Method/catalyst	Degradation efficiency	Additional conditions	Reference
Thermal-assisted activation PMS/ Co-N/C@CeO_2	92.3%	Pre-treated at 180 °C, 55 °C, 5 mM PMS, 1 mL H_2O_2 in 100 mL H_2O, 6 h	[1]
Photocatalysis/C,N-TiO_2	70%	0 °C, pH=3	[2]
Photocatalysis/KPF_6/BiOBr	26%	Isopropanol as sacrificial agent, pH=2	[3]
Photocatalysis/ $NiAl_2O_4$	12.50%	Using DMSO as solvent	[4]
Bacterial enzyme cascade reaction/*Escherichia coli*	21.4%	pH = 3, 30 °C, 168 h	[5]
Electrolysis& H_2O_2/C/TiO_2-graphite cathode	75%	O_2 saturated atmosphere, and pH=3.0, 100 °C	[6]
Piezoelectricity& Fenton-like/ BCFO	39.2%	/	This work

Table S2 Degradation efficiency of MPs by various ultrasound-assisted systems.

Ultrasonic power and frequency/catalyst	MPs/Conc-entration (g L^{-1})	Time (h)	Degradation efficiency	Additional conditions	Reference
650 W&35 kHz/ MXene@MIL-125(Ti)	PE/0.5	4	78.0%	/	[7]
600 W&40 kHz/ Ce_3Mn_7-PbO_2 anode	PET/0.1	6	45.9%	electrocatalytic	[8]
200 W&580 kHz/ /	PTFE/0.04	46	~100%	5 g L^{-1} sodium dodecyl sulfate	[9]
200 W&20 kHz / /	DEHP/ /	24	41.7%	pH=10, n_{DEHP}:n_{H2O2}=1:1	[10]
120 W&40 kHz/ BCFO	PET/3	40	39.2%	250 mM H_2O_2	This work
	PP/3		14.0%		
	PE/3		37.0%		

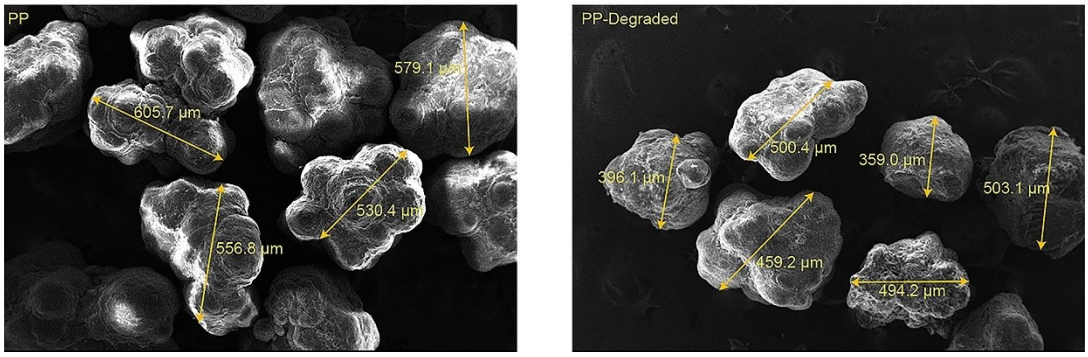

Fig. S6 SEM images of original and degraded PP-MPs.

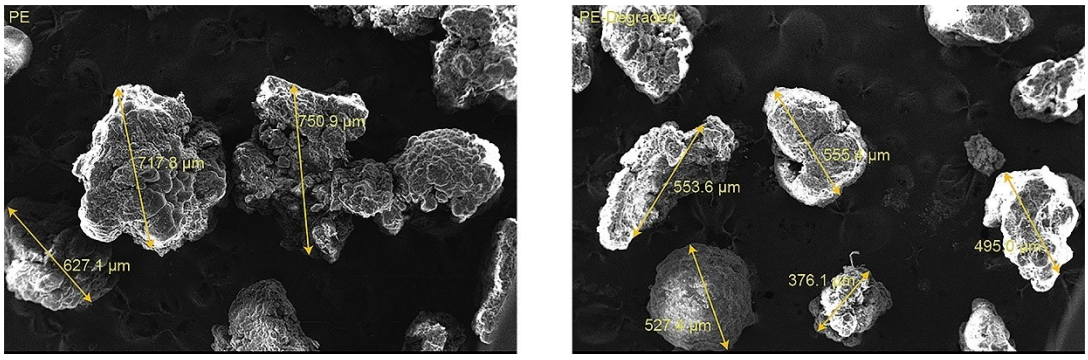

Fig. S7 SEM images of original and degraded PE-MPs.

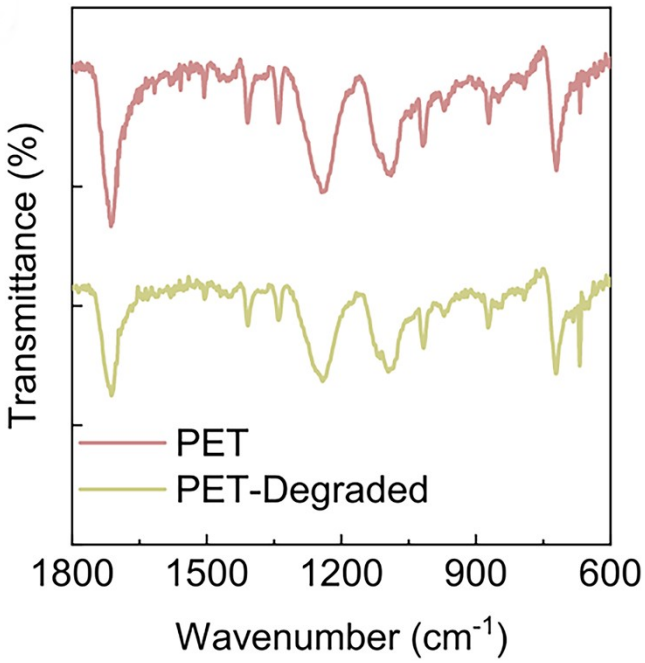

Fig. S8 ATR-FTIR spectra of original and degraded PET-MPs.

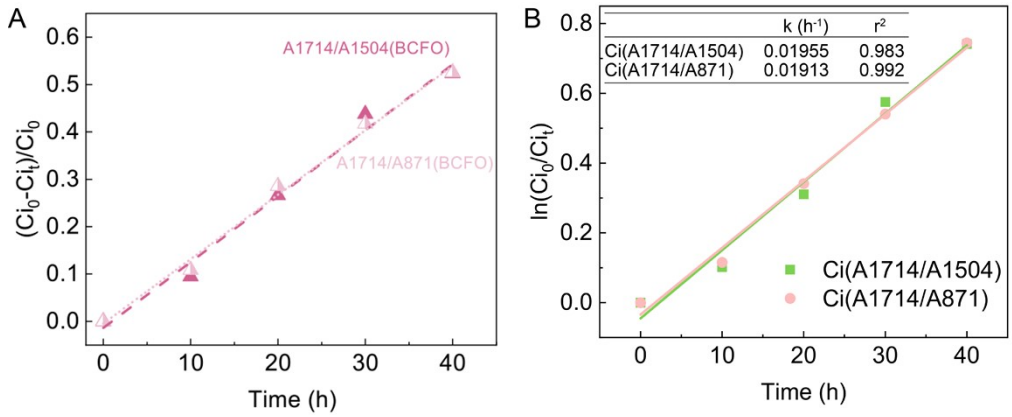

Fig. S9 (A) Carbonyl index removal efficiency during PET-MPs degradation, (B) Quasi-first-order dynamic fitting of PET-MPs based on Ci.

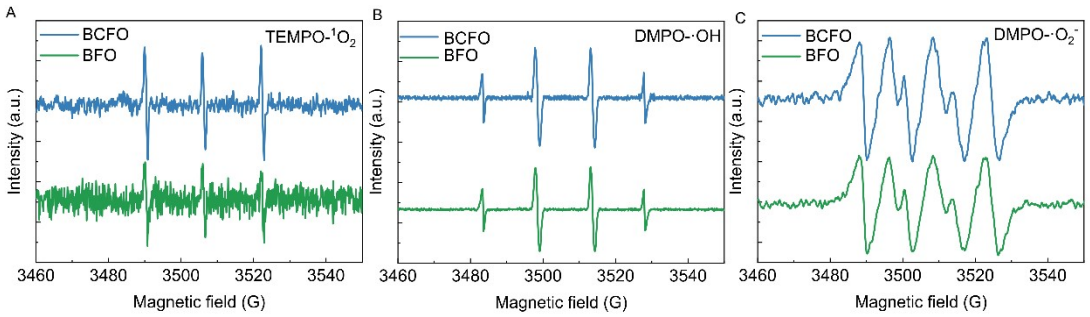

Fig. S10 EPR examination for the detection of (A) $^1O_2$, (B) ·OH and (C) ·O_2^-.

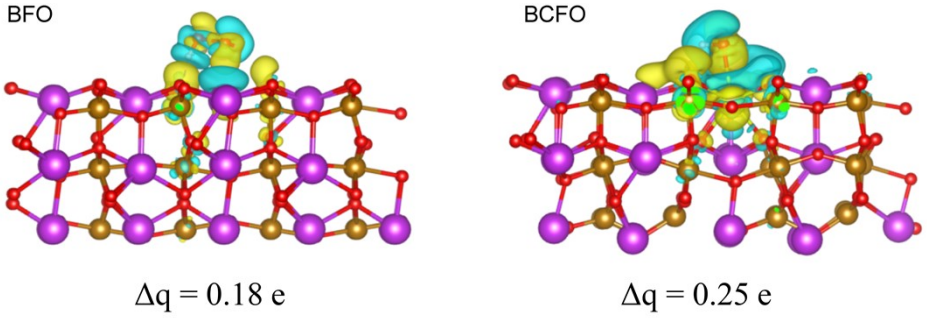

Fig. S11 Differential charge (Δq) of BFO and BCFO.

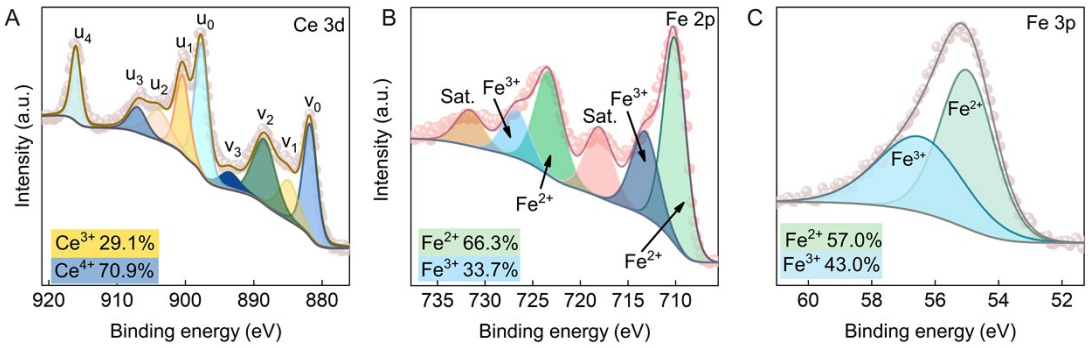

Fig. S12 High-resolution (A) Ce 3d; (B) Fe 2p; and (C) Fe 3p spectra of recycled BCFO.

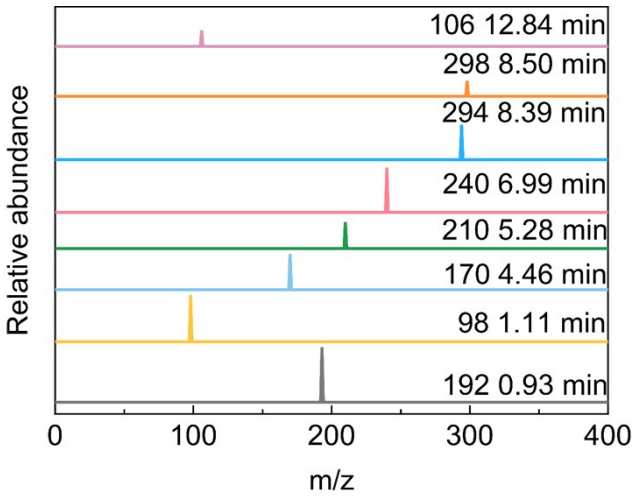

Fig. S13 Mass spectrum of the intermediates during the degradation of PET-MPs.

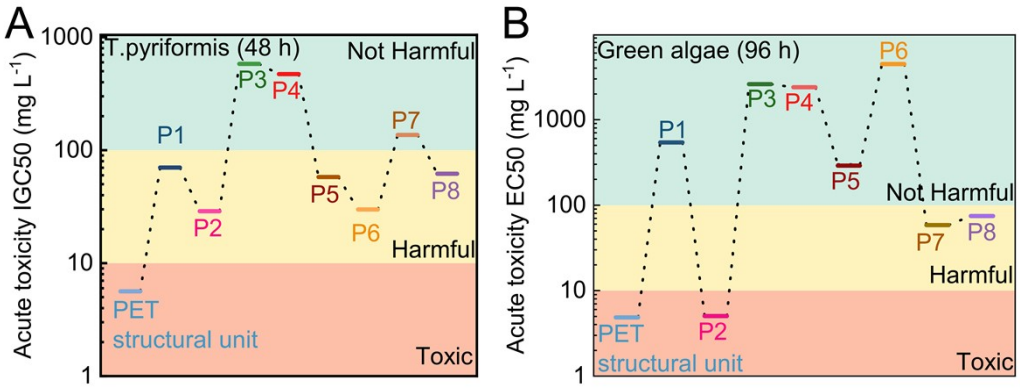

Fig. S14 Toxicity assessments of intermediate products during PET-MPs degradation acute toxicity for (a) T. pyriformis and (b) Green algae.

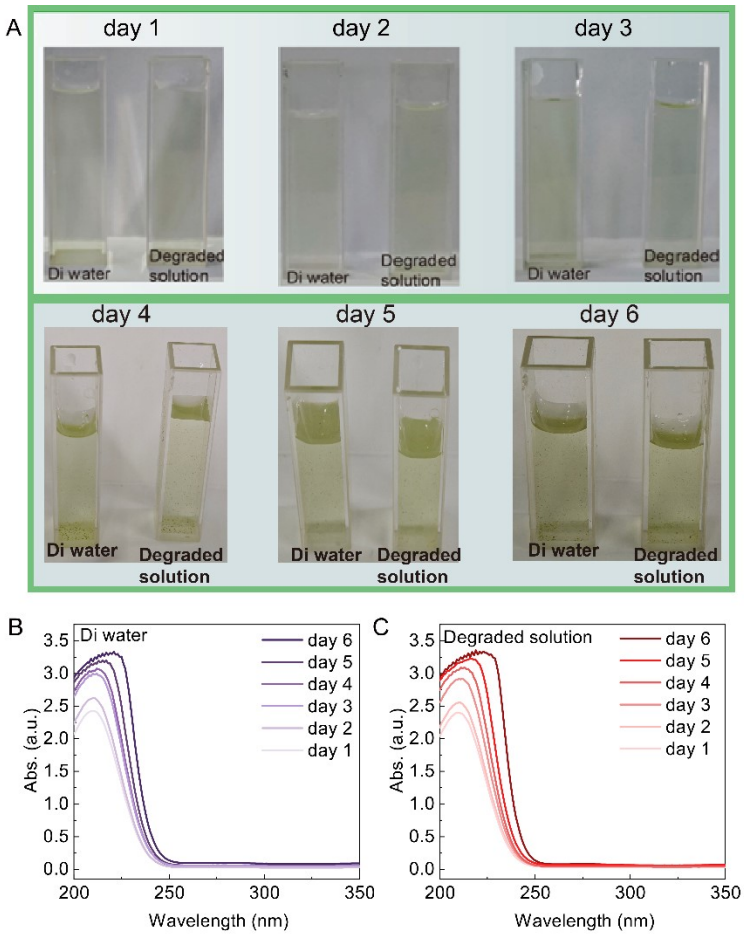

Fig. S15 (A) Photographic images and (B, C) absorbance of Chlorella in Di water and in degraded solution.

Reference

[1] Wang, H. J.; Chen, H. Z.; Wan, Q. Q.; Zheng, Y. Z.; Liu, X.; Song, X. S.; Ma, W.; Hou, P. W.; Catalytic degradation of polyethylene terephthalate microplastics by Co-N/C@CeO_2 composite in thermal-assisted activation PMS system: Process mechanism and toxicological analysis. Chemical Engineering Journal **2025**, *514*, 163192.

[2] Tarazona, M. C. A.; Chiu, J. F. V.; López, J. M. H.; la Rosaa, J. R. D.; Barbieric, V.; Siligardi, C.; Cedillo-González, E. I.; Microplastic pollution reduction by a carbon and nitrogen-doped TiO_2: effect of pH and temperature in the photocatalytic degradation process. Journal of Hazardous Materials **2020**, *395*, 122632.

[3] Du, C. W.; Feng, W. W.; Nie, S. Y.; Zhang, J. L.; Liang, Y. T.; Han, X.; Wu, Y. H.; Feng, J. L.; Dong, S. Y.; Liu, H. J.; Sun J. H.; Harnessing efficient in-situ H_2O_2 production via a KPF_6/BiOBr photocatalyst for the degradation of polyethylene. Separation and Purification Technology **2021**, *279*, 119734.

[4] Venkataramana, C.; Botsa, S. M.; Shyamala, P.; Muralikrishna, R.; Photocatalytic degradation of polyethylene plastics by $NiAl_2O_4$ spinels-synthesis and characterization. Chemosphere **2021**, *265*, 129021.

[5] Wang, C.; Long, R.; Lin, X.; Liu, W.; Zhu, L.; Jiang, L.; Development and characterization of

a bacterial enzyme cascade reaction system for efficient and stable PET degradation. Journal of Hazardous Materials **2024**, *472*, 134480.
[6] Miao, F.; Liu, Y. F.; Gao, M. M.; Yu, X.; Xiao, P. W.; Wang, M.; Shuguang Wang, S. G.; Wang X. H.; Degradation of polyvinyl chloride microplastics via an electro-Fenton-like system with a TiO_2/graphite cathode. Journal of Hazardous Materials **2020**, *399*, 123023.
[7] Yang, F. F.; Li, J. L.; Dong, J.; Chen, S. Y.; Hu, W. Y.; Zhang, Y. F.; Wang, H. Q.; Li, Z. F.; Wang, Z. H.; MX@MIL-125(Ti)-mediated sonocatalytic degradation for the dyes and microplastics. Separation and Purification Technology **2024**, *337*, 126488.
[8] Duan, X. Y.; Ning, Z. Q.; Sui, X. Y.; Geng, S. Y.; Wang, H. L.; Liu, C. B.; Chang, L. M.; Ultrasound-assisted electrocatalytic degradation of microplastics by a hydrophobic Ce_3Mn_7-PbO_2 anode: Enhanced performance and degradation mechanism. Journal of Environmental Chemical Engineering **2025**, *13*, 116207.
[9] Pu, R. Q.; Zhao, L. R.; Deng, S. H.; Naidu, R.; Mantzavinos, D.; Lin, L. L.; Fang, C.; Lei, Y. J.; Effect of high-frequency ultrasonication on degradation of polytetrafluoroethylene (PTFE) microplastics/nanoplastics. Separation and Purification Technology **2025**, *357*, 130229.
[10] Kida, M.; Ziembowicz, S.; Koszelnik, P.; The Use of an Ultrasonic Field in Support of Classical Methods of Oxidising Component Leached from Microplastics in Bottom Sediments. Materials **2021**, *14*, 3029.